Origin of Al deficient Ti_2AlN and Pathways of Vacancy-assisted Diffusion

Zheng ZHANG,[†] *Hongmei JIN,**[‡] *Jisheng PAN,*[†] *Jianwei CHAI,*[†] *Lai Mun WONG,*[†] *Michael B. SULLIVAN,*[†] *and Shi Jie WANG***[†]

[†]Institute of Materials Research and Engineering, A*STAR (Agency for Science, Technology and Research), 3 Research Link, 117602, Singapore.

[‡]Institute of High Performance Computing, A*STAR (Agency for Science, Technology and Research), 1 Fusionopolis Way, Connexis, 138632, Singapore.

ABSTRACT

To understand the origin of Al-deficient Ti_2AlN MAX phase observed in our experiments, formation and diffusion pathway of Al vacancy in Ti_2AlN have been calculated by density functional theory (DFT). Compared to Ti and N vacancies, Al vacancy requires the lowest formation energies not only in the bulk but also at top surface layer and second surface layer. As a result, Ti_2AlN is calculated to be capable of accommodating Al vacancies in the supercell down to a sub-stoichiometric $Ti_2Al_{0.75}N$ while maintaining the MAX phase structure. After the vacancy formation, Al atom is calculated to diffuse along the (0001) plane preferentially via vacancy jump with an energy barrier of 0.80 eV, leading to Al surface segregation and subsequent desorption from Ti_2AlN at high temperatures.

Keywords: Ti_2AlN, MAX Phase, Vacancy, Diffusion, Density functional theory

I. Introduction

$M_{n+1}AX_n$ (M: an early transition metal, A: an element in groups IIA and IVA, X: N and/or C, n=1-3) or MAX phase materials are a family of about 60 nanolaminate ternary compounds, which exhibits interesting combination of ceramic properties (lightweight, refractory and elastically stiff) and metallic properties (electrical and thermal conductive, machinable and thermal-shock resistant).[1-2] Such special properties are associated with their complex hexagonal structure based on a unit cell comprised of twinned $M_{n+1}X_n$ layers interleaved by one A element layer. The strong covalent-ionic M-X bonds contribute to ceramic properties, while the weak metallic M-A bonds contribute to metallic properties.[1-2] Some well-studied MAX phase materials include Ti_3SiC_2, Ti_2AlC, etc.

The bulk MAX phase materials were synthesized by hot isostatic pressing (HIP) at high temperature (>1000^oC) and at high pressure (>20MPa) or by self-propagating high-temperature synthesis (SHS) of M-A-X or MX-A or MX-AX powders.[1-2] Additional A-containing powders usually need be added to the starting powders in order to achieve the stoichiometric $M_{n+1}AX_n$.[3-6] It is because A elements, such as aluminum (Al), tend to evaporate more easily as compared to M elements and usually result in a loss of A elements at high temperatures. Due to the same reason, the MAX phase thin films, i.e., Ti_2AlC,[7] Ti_3SiC_2,[8] V_2GeC[9] and Ti_2SnC,[10] deposited by direct current (DC) sputtering are often reported to be A-deficient in compositions. However, these non-stoichiometric thin films are still able to maintain the characteristic hexagonal MAX phase structure, which indicates that MAX phase materials are capable of accommodating certain degrees of structural defects like vacancy. Such defect-tolerance capabilities have led to investigation of MAX phase materials (Ti_3AlC_2[11] and Ti_3SiC_2[11-12]) under high energy heavy ions

(Au, Kr and Xe) radiation and exploration of their application as cladding material for future nuclear fuel. Very recently, both Ti_2AlC and Ti_2AlN have been subjected to investigation of their radiation tolerance theoretically by first-principle calculation[13] and experimentally by Ar^{2+} ion and neutrons irradiation[14-15]. It has been predicted by the calculation that the Ti_2AlC and Ti_2AlN are the most two competent MAX phases in tolerating radiation damage,[13] while experiments show that Ti_2AlN indeed withstands 100 keV Ar^{2+} ion irradiation[14] and 0.1 displacement per atom of neutron radiation[15]. Similar to mechanism behind radiation tolerance of ternary spinel oxide (i.e., $MgAl_2O_4$) and pyrochlore oxides $A_2B_2O_7$ (A & B are metallic cations, i.e., $Er_2Zr_2O_7$),[16] these MAX phase materials with their complex chemistry and lattice structures are likely to have inherent propensity to accommodate certain amount of lattice defects (i.e., vacancy, interstitials, antisites, displacements, etc.) before these defects accumulate beyond a critical size, form dislocation loop nucleus and amorphize the whole structure.

We have recently deposited thin films of one MAX phase material, Ti_2AlN, on MgO(111) substrates using DC sputtering at 750 ^{o}C.[17] The atomic composition of Al probed by *in-situ* X-ray photoelectron spectroscopy (XPS) varies between 10.9 to 27.7 % as shown in Fig. 1(a). Although Al % is mostly below its stoichiometric value of 25 %, indicating formation of Al-deficient sub-stoichiometric Ti_2Al_xN, both transmission electron microscopy (TEM) and X-ray diffraction (XRD) have revealed the single crystalline nature of the resulting MAX phase thin films.[17] When these single crystalline Ti_2Al_xN thin films were annealed in the ultra-high-vacuum analysis chamber of XPS with base pressure of 1.0×10^{-9} mbar, Al was observed to preferentially segregate to surface at 700 ^{o}C and desorbed heavily from the thin film above 800 ^{o}C (Fig. 1(b)).[18] At 900 ^{o}C, Al % decreased to as low as 4.3 %. Loss of Al, which was further supported by energy dispersive X-ray spectroscopy (EDS) and time-of-flight secondary ion mass

spectroscopy (TOF-SIMS) depth profiling, resulted in decomposition of Ti_2Al_xN MAX phase into a mixture of polycrystalline δ-TiN_{1-x} and ξ-$TiN_{0.75-y}$ phases.

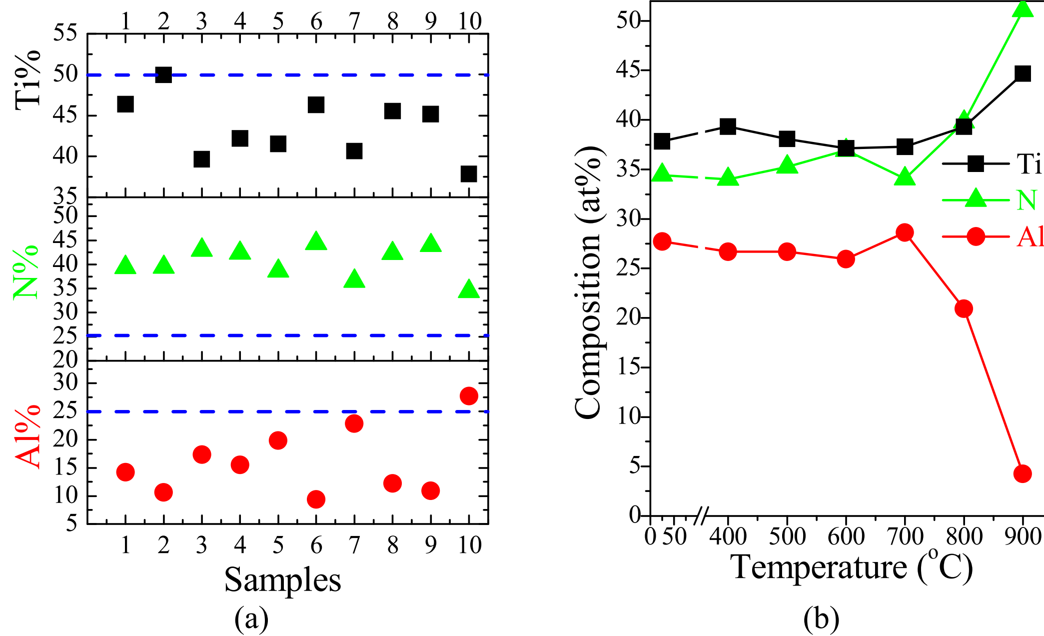

Fig. 1 (a) Atomic composition of Ti, N and Al in ten single crystalline Ti_2AlN samples. The blue dash lines represent the stoichiometric values of Ti, N and Al in Ti_2AlN. (b) Change of Ti, N and Al atomic composition after annealing the 400 nm single crystalline Ti_2AlN thin film in the ultra-high-vacuum analysis chamber of XPS.

Ti_2AlN shares a similar structure as Ti_2AlC, except that the nitrogen (N) positions were replaced by carbon (C). Ti_2AlC thin films deposited by DC sputtering have also been reported to be Al-deficient in composition, especially at high temperatures.[7] Al has also been observed to preferentially segregate out and is oxidized into a continuous inner protective Al_2O_3 layer below a discontinuous outer TiO_2 layer.[19-20] This continuous inner Al_2O_3 scale helps prevent further oxidation of Ti_2AlC at underneath. These observations have been explained by the low Al vacancy formation energy of 2.73 eV and low Al self-diffusion energy barrier of 0.83 eV along the (0001) plane calculated by first-principles theory, leading to rapid out-diffusion of Al

observed at high temperatures and during oxidation.[21-23]

Similar to the behavior of Al in Ti_2AlC, we have observed the formation of Al vacancy and the preferential out-diffusion of Al in Ti_2AlN thin films as described earlier. However, there are very limited theoretical studies pertaining to the vacancy formation inclination in Ti_2AlN. To the best of our knowledge, only recently is there one such calculation which predicts Al mono-vacancy is most energetically favorable in Ti_2AlN but does not give its threshold concentration value.[24] Another $Ti_{n+1}AlN_n$ MAX phase material, Ti_4AlN_3, has been reported experimentally having slightly sub-stoichiometric in N instead[25] and calculated to be energetically favorable to have N vacancies by density functional theory (DFT).[26] Therefore, in this paper, we investigate the formation of Ti, Al and N vacancies in Ti_2AlN as well as the possible vacancy-assisted diffusion pathways through DFT calculations. We will show that formation of Al vacancy is energetically more favorable than the formation of Ti and N vacancies due to its lower formation energy. In addition, the energy barriers for Al diffusion via vacancy exchange along and across Al planes have also been investigated and compared. This study will help us understand the origin of a non-stoichiometric yet stable Ti_2AlN MAX phase material and the Al atoms' migration pathways during high temperature oxidation or annealing.

II. Calculation methods

All the vacancy formation energies and structure stability calculations were performed with Vienna ab initio simulation package (VASP).[27] The generalized gradient approximation (GGA-PBE)[28] scheme is used for electron exchange and correlation, while the frozen-core projector augmented wave (PAW) method is used to describe the interaction between ions and electrons.[29] A plane wave cut-off of 500eV was employed and Brillion-zone integration was

performed on a Monkhorst-Pack grid (2 × 2 × 1 for surface slab model, and 1 × 1 × 1 for vacancy and stability calculations). The structure was relaxed until the convergence of Hellmann-Feynman forces was less than 0.01 eV/Å per atom. For diffusion barrier calculations, we used both of Nudged Elastic Band (NEB) method which was implemented in VASP and LST/QST method. The LST/QST was implemented in the CASTEP module of Accelrys simulation package.[30] The Al diffusion barrier along (0001) plane is calculated to be 0.80eV with CASTEP and 0.70eV with VASP, showing comparable results by the two calculation methods. For convenience, the diffusion barriers along the *z* directions were thus evaluated with CASTEP.

III. Results and discussion

A. Formation of neutral mono-vacancy

In order to validate both the pseudopotentials and the methods used in this work, we have calculated the lattice constants (*a* and *c*), bulk and Young's modulus of the perfect Ti_2AlN using a unit cell with 8 atoms to be 2.994 Å, 13.64 Å, 150 GPa and 277 GPa, respectively. These results are comparable with both of experimental results and other theoretical calculations.[1, 31-32] We thereafter calculate the formation of mono-vacancies inside the bulk Ti_2AlN in a 4 × 4 × 1 cell with a total of 128 atoms. Note that vacancy formation energy strongly depends on the vacancy's concentration (or supercell size) and hence a large supercell is adopted for a better accuracy. The formation energy E_V^A of a neutral vacancy in Ti_2AN can be calculated through:

$$E_V^A = E_{Def}^A - E_{Per} + \mu_A^0 \tag{1}$$

where E_{Def}^A is the total energy for a supercell containing a neutral vacancy of A (A = Ti, Al or N)

atom, E_{Per} is the total energy for a defect-free perfect supercell, and μ_A^0 is the A element's chemical potential which varies depending on the chemical environment of the system. The chemical potential of three elements should be correlated to each other in order to satisfy the following equation:

$$2\mu_{Ti} + \mu_{Al} + \mu_{N} = \mu_{Ti_2AlN(bulk)} \tag{2}$$

Fig. 2 shows the schematic phase diagram of Ti-Al-N. The vertices of the triangle denote the chemical potential for the formation of corresponding elemental solid, while the competing phases considered are illustrated on the three sides of the triangle based on their stoichiometric proportion. Points A to F denote the 6 possible chemical potential combinations, while the hexagon formed by intersection of these six points defines the thermodynamically equilibrium region of the ternary Ti-Al-N system. For example, at point B and C, the system represents an N-rich environment, while at point E and F, the system is at N-poor environment instead.

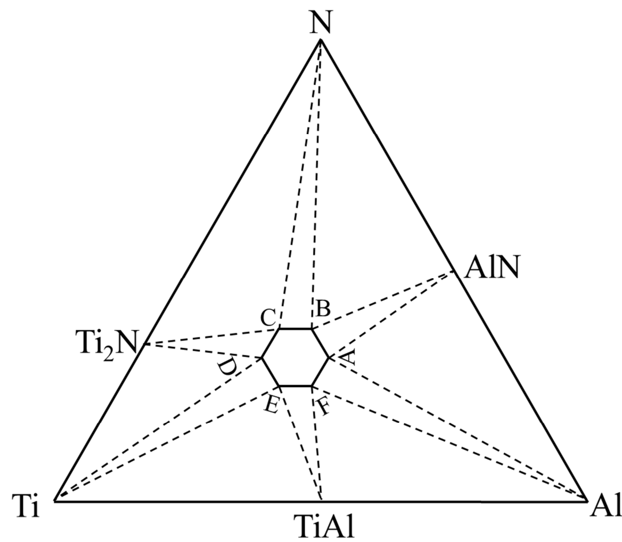

Fig.2 Schematic phase diagram of the ternary system Ti-Al-N. The central hexagon represents the stable region of Ti_2AlN for certain elemental chemical potentials described by Equation 3.

At each vertex of the hexagon in Fig. 2, the chemical potentials of each element can be described by the following equations:

point A : $\mu_{Al} = \mu_{Al(bulk)}$ $\mu_{N} = \mu_{AlN(bulk)} - \mu_{Al}$ $\mu_{Ti} = \frac{1}{2}(\mu_{Ti_2AlN(bulk)} - \mu_{Al} - \mu_{N})$ (3a)

point B : $\mu_{N} = \mu_{N(bulk)}$ $\mu_{Al} = \mu_{AlN} - \mu_{N}$ $\mu_{Ti} = \frac{1}{2}(\mu_{Ti_2AlN(bulk)} - \mu_{Al} - \mu_{N})$ (3b)

point C: $\mu_{N} = \mu_{N(bulk)}$ $\mu_{Ti} = \frac{1}{2}(\mu_{Ti2N} - \mu_{N})$ $\mu_{Al} = (\mu_{Ti_2AlN(bulk)} - 2\mu_{Ti} - \mu_{N})$ (3c)

point D: $\mu_{Ti} = \mu_{Ti(bulk)}$ $\mu_{N} = \mu_{Ti2N} - 2\mu_{Ti}$ $\mu_{Al} = (\mu_{Ti_2AlN(bulk)} - 2\mu_{Ti} - \mu_{N})$ (3d)

point E: $\mu_{Ti} = \mu_{Ti(bulk)}$ $\mu_{Al} = (\mu_{TiAl} - \mu_{Ti})$ $\mu_{N} = (\mu_{Ti_2AlN(bulk)} - 2\mu_{Ti} - \mu_{Al})$ (3e)

point F: $\mu_{Al} = \mu_{Al(bulk)}$ $\mu_{Ti} = (\mu_{TiAl} - \mu_{Al})$ $\mu_{N} = (\mu_{Ti_2AlN(bulk)} - 2\mu_{Ti} - \mu_{Al})$ (3f)

Chemical potential of the bulk substances in these equations were obtained as the total energies per formula unit by separate calculations. For example, bulk structure of Ti (p63/mmc), Al (fcc), Ti_2N (p42/mnm), TiAl (p4/mmm), AlN (p63/mc) and Ti_2AlN (p63/mmc) were used to determine their respective chemical potentials, while the chemical potential of N was calculated from the total energy of N_2 molecule by using a big box with spin polarized calculations. The results are shown in Table 1.

Table 1 Calculated chemical potentials of Ti, Al, N, Ti_2N, TiAl, AlN and Ti_2AlN

System	Chemical potential (in eV)
Ti	-7.89
Al	-3.75
N	-8.31
Ti_2N	-27.29
TiAl	-12.44
AlN	-14.89
Ti_2AlN	-32.21

The resultant vacancy formation energies at the six vertices of hexagon defined in Fig.2 are summarized in Table 2 and plotted in Fig.3 for easy visualization. According to the results shown in Table 2 and Fig.3, under N-rich environment (i.e., point B), the vacancy formation energy of Al is the lowest (2.09 eV), followed by that of Ti (5.16 eV) and is the highest for that of N (6.64 eV). But under N-poor environment (i.e., point E), the vacancy formation energy of N is the lowest (3.07 eV), compared to the vacancy formation energies of Al (4.11 eV) and Ti (5.93 eV). N% has been reported to plays a key role for the phase formation of Ti_2AlN and the critical N% value is in the range of 22.5 ~ 29.6 %,[33] which suggests the likelihood of presence of both N-rich and N-poor Ti_2AlN. While Dolique *et al*[34] and Acabarozi *et al*[35] observed a N-poor Ti_2AlN, the single crystal Ti_2AlN thin films we deposited in the narrow N_2 partial pressure window are N-rich (Fig. 1(a)), which has also similarly been observed in most experimental conditions by T. Joelsson *et al*[36], M. Beckers *et al*[37] and P. Persson *et al*[38]. In such N-rich Ti_2AlN structure, Al vacancy is most likely to be the dominant vacancy specie due to its lowest formation energy in bulk Ti_2AlN. Duan *et al* has similarly predicted that Al mono-vacancy has the lowest formation energy of 3.02 eV in Al-rich Ti_2AlN through DFT calculation.[24] It is worth noting that the Al vacancy formation energy in the bulk is generally higher in Ti_2AlN (2.09 ~ 4.92 eV) compared to that in Ti_2AlC (2.73 eV).[21] This can be explained by the shorter Ti-Al bond order in Ti_2AlN (0.153) than that in Ti_2AlC (0.159) and hence a stronger Ti-Al bonding in Ti_2AlN than in Ti_2AlC.[39] As a result, it is slightly more difficult to break Ti-Al bonds in Ti_2AlN than in Ti_2AlC to form an Al vacancy as it requires larger vacancy formation energy.

Table 2 Formation energies of neutral Ti, Al and N vacancies (E_V, in eV) at the six vertices of hexagon denoted in Fig. 2

Vertex	E_V(Ti)	E_V(Al)	E_V(N)
A	5.16	4.92	6.64
B	5.16	2.09	6.64
C	4.33	3.75	6.64
D	5.93	3.75	3.44
E	5.93	4.11	3.07
F	5.12	4.92	3.88

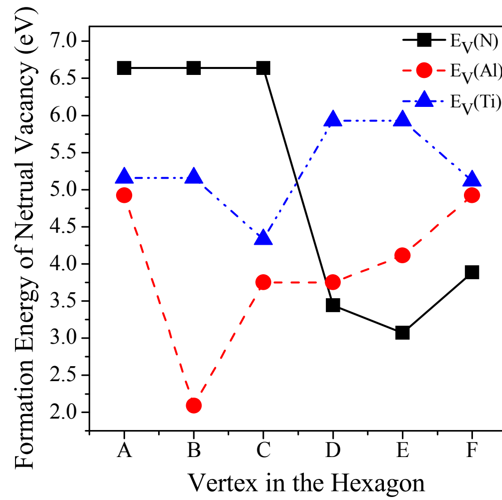

Fig. 3 Formation energies of Ti, Al and N neutral vacancies at the six equilibrium vertices labeled as A to F in Ti–Al–N ternary phase diagram as shown in Fig. 2.

Besides comparing the vacancy formation energy in the bulk, the vacancy formation energy on the surface region was also evaluated, which was carried out by employing slab models with a 15 Å vacuum as shown in Fig. 4. The vacancy was considered to be created on the top and second layers respectively for each type of atom. The total energies of the slabs with and without vacancies were fully relaxed and the vacancy formation energy of each element was derived according to Equation (1) by assuming that the chemical potential of each element is equal to its corresponding bulk chemical potential. The calculation results in Table 3 suggest that

the vacancy formation energies of one atom are lower on the top layers than on the second layers, which are further lower compared with the bulk vacancy formation energies (Table 2). This is expected as the vacancies near free surface require fewer amounts of bonds to be broken. In addition, the vacancy formation energy of Al is smallest comparing to those of Ti and N, regardless of whether it is on top or on the second layer. The DFT calculation has thus demonstrated that formation of Al vacancies requires the smallest energies compared to those of Ti and N not only at the surface layer but also in the bulk, which suggests that Al vacancy should be the dominant and preferable vacancy species to be formed in Ti_2AlN. As such, we will focus our subsequent calculation on Al vacancies only.

Table 3 Calculated formation energies of Ti, Al and N vacancies created in the top surface layer and second layer using slab models. Ti_1 and Ti_2 represent Ti atoms at two different positions connecting directly with Al and N atoms, respectively

Vacancy type	E_V^A in surface layer (top layer) (eV)	E_V^A in second layer (eV)
Ti_1-vacancy	1.84	3.70
Ti_2-vacancy	1.42	3.62
Al-vacancy	1.05	2.70
N-vacancy	1.57	4.37

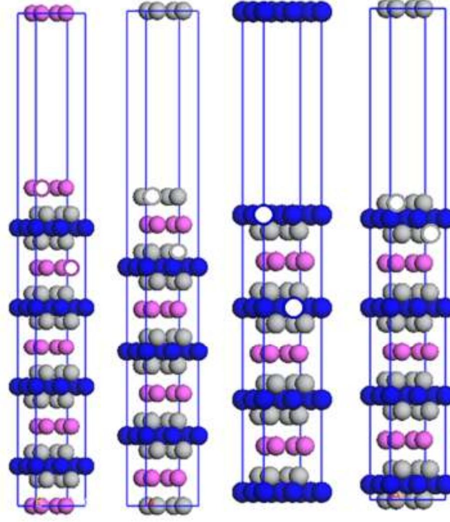

Fig. 4 Four slab models representing four structures with the top surface layer terminated by Al (pink), Ti_1 (grey), N (blue) and Ti_2 (grey) from left to right. Ti_1 and Ti_2 represent Ti atoms at two different positions connecting directly with Al and N atoms, respectively. The respective vacancies at top layer and second layer are illustrated by the corresponding hollow circles.

B. Stability of Al-deficient Ti_2Al_xN

Since both the experiment and DFT calculation of vacancy formation energy suggest the formation of an Al-deficient Ti_2Al_xN, it is important to further probe the threshold limit of the Al deficient content before the whole structure becomes unstable. We consider that the phase stability is determined by the energetic competition of sub-stoichiometric Ti_2Al_xN ($E_{Ti_2Al_xN}$) with respect to the twinned Ti_2N (E_{Ti_2N}) and elemental Al (μ_{Al}^0). The formation energy ($E_{Formation}$) of Ti_2Al_xN under different Al contents can be estimated according to the following equation:

$$E_{Formation} = E_{Ti_2Al_xN} - E_{Ti_2N} - x\mu_{Al}^0 \quad (4)$$

A negative $E_{Formation}$ suggests that the sub-stoichiometric Ti_2Al_xN is stable, while a positive

value indicates that Ti_2Al_xN is unstable and may decompose. The formation energy was evaluated by gradually removing 2, 4, 6, 8, 9, 10 and 12 Al atoms out from the top Al layer of a perfect 4 × 4 × 1 Ti_2AlN supercell (the removal process is shown schematically in Fig. S1 of the supporting information). It is because the top Al layer is close to free vacuum surface, and thus requires the lowest energy and should be the easiest to be removed. The results (Table 4) suggest that the sub-stoichiometric Ti_2Al_xN can still maintain its phase stability down to $Ti_2Al_{0.75}N$ by removing 8 or 25% out of a total of 32 Al atoms. This corresponds to a threshold Al % of 20 % (with 53.3 %Ti and 26.7 %N), which explains why the Al-deficient Ti_2Al_xN thin film we deposit at 750 ^oC can still maintain the single crystalline structure below its stoichiometric value of 25%. It is worth noting that the Al% detect by XPS is between 10.9 to 27.7%, most of which (Fig. 1(a)) is lower than the 20% predicted by DFT calculation. The difference may be attributed to the variation caused by temperature factor: the DFT calculation simulates the structure stability at absolute zero degree while the actual deposition takes place at 750 ^oC. The high temperature and the resultant high thermal energy can lead to a high degree of vibration and movement of Al atoms, which can cause a greater loss of Al from the structure at high temperature. This threshold limit is less than 50% of Al that Ti_2AlC can afford to lose before the sub-stoichiometric Ti_2Al_xC becomes energetically unstable.[21] The difference is also likely attributed to stronger Ti-Al bond in Ti_2AlN than in Ti_2AlC which prevents Al from breaking bonds with Ti to form a free Al atom and then the Al vacancy.[39]

Table 4 Formation energy ($E_{Formation}$, in eV) of sub-stoichiometric Ti_2Al_xN after removing 2, 4, 6, 8, 9, 10 and 12 Al atoms from a 4 × 4 × 1 Ti_2AlN supercell calculated by Equation (4).

Stoichiometry	Number of Al Removed	$E_{Formation}$ (eV)
Ti_2AlN	0	-20.878
$Ti_2Al_{0.9375}N$	2	-16.106
$Ti_2Al_{0.875}N$	4	-11.436
$Ti_2Al_{0.8125}N$	6	-6.416
$Ti_2Al_{0.75}N$	8	-2.126
$Ti_2Al_{0.7187}N$	9	0.184
$Ti_2Al_{0.6875}N$	10	2.044
$Ti_2Al_{0.625}N$	12	3.774

While the structure of sub-stoichiometric Ti_2Al_xN can remain stable, it would be interesting to examine the development of the electronic structure with respect to a gradual depletion of Al from Ti_2AlN. The total density of states (TDOS) and partial density of states (PDOS) of Ti, Al and N of a perfect 4 × 4 × 1 Ti_2AlN supercell and after removing 2 and 9 Al atoms are calculated and selected to show in Fig. 5. A complete display of TDOS and PDOS after removing 2, 4, 6, 8 and 9 Al toms can be found in Fig. S2 & S3 of the supporting information. Compared to the less significant changes in the PDOS of Ti and N (Fig. 5(a) and (c)), there was a decrease of the Al PDOS at between Fermi Level (E_F, 0eV) and -8 eV region with an increase in the removal of Al atoms from 2 to 9 (Fig. 5(b)). This is understandable as PDOS of Al at this region is contributed by Al 3*p* (mainly) and Al *3s* states.[17] A decrease in the number of Al atoms remaining in the structure thus leads to a decrease in PDOS of Al at this region. Accordingly, the TDOS (Fig. 5(d)) from -0.5 to -2.0 eV also shows a decrease with continuous removal of Al atoms, because the TDOS at this range is contributed mainly by Ti 3*d*-Al 3*p* hybridization. The development in electronic structure after progressive removal of Al atoms suggests a likely increase in electrical resistivity of sub-stoichiometric Ti_2Al_xN as a result of reducing number of Al atoms and hence the Al density in the Ti_2Al_xN. Experimentally, it has been observed that the electrical resistivity

increased in $Ti_{n+1}GeC_n$ (from 15-20 μΩ cm for Ti_2GeC to 50 μΩ cm for Ti_3GeC_2) and $Ti_{n+1}SiC_n$ (from 27 μΩ cm for Ti_3SiC_2 to 51 μΩ cm for Ti_4SiC_3) MAX phase systems with decreasing respective A-element layer's density.[10]

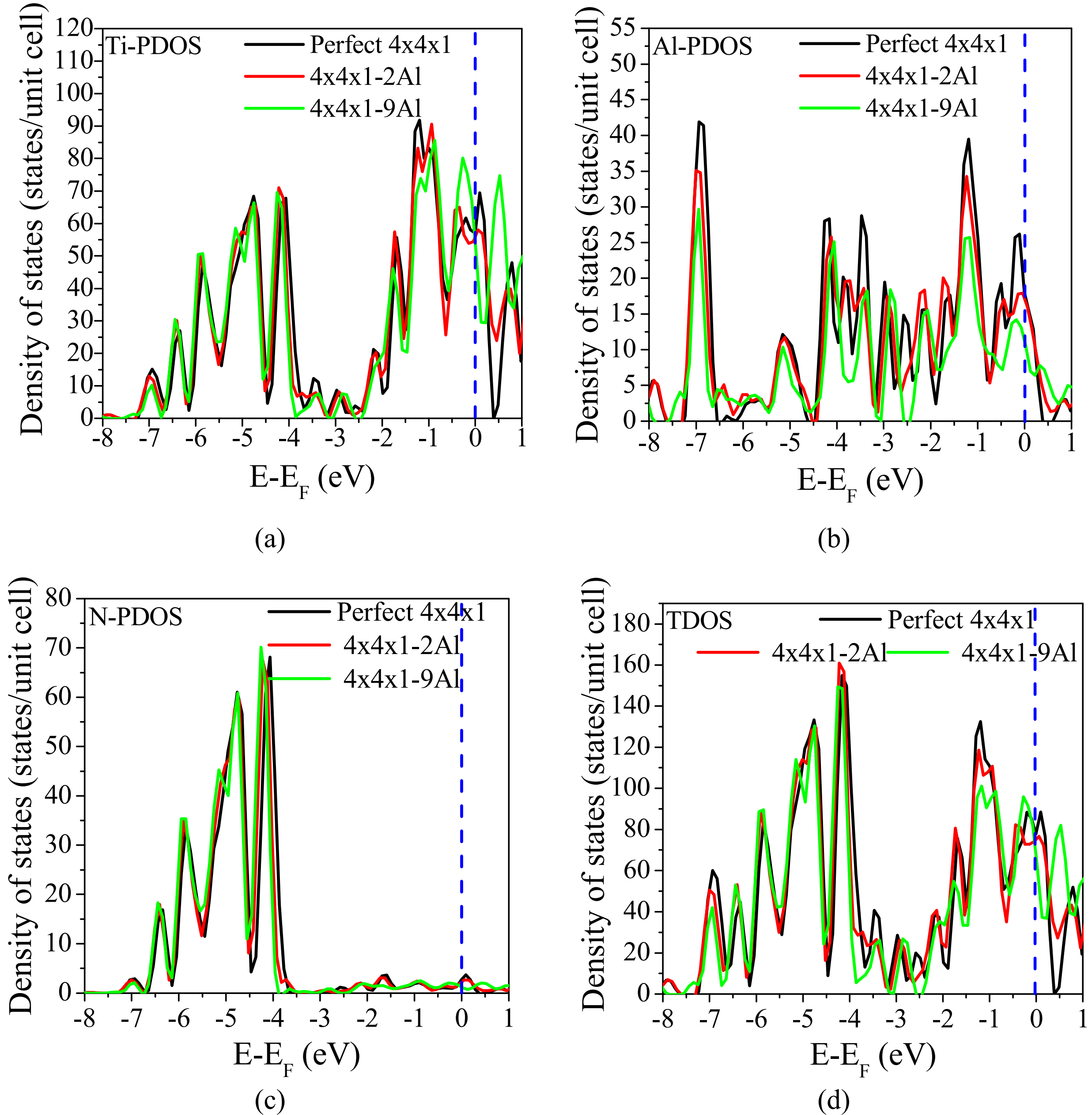

Fig.5 Partial density of states (PDOS) of (a) Ti, (b) Al, (c) N and (d) total density of states (TDOS) from a perfect 4 × 4 × 1 Ti_2AlN supercell (black) and a sub-stoichiometric Ti_2Al_xN after removing 2 (red) and 9 (green) Al atoms from the supercell.

An Al vacancy will be created after an Al atom jumps out of its lattice position. This

vacancy will facilitate an Al atom nearby exchanging its position either with the vertical adjacent Ti/N layer or with Al atoms in the same horizontal layer. Both exchanges may assist the diffusion of atoms vertically or horizontally, depending on the diffusion barrier. To investigate the diffusion of Al atoms along and across (0001) or *xy*-plane via vacancy jump, we evaluate the diffusion barrier using a $2 \times 2 \times 1$ supercell in the next section.

C. Al Vacancy Diffusion Pathway

We started off by calculating the Al atom diffusion barrier along the (0001) or *xy*-plane through self-diffusion mechanism by exchanging with a neighboring Al vacancy in the same plane in Ti_2AlN (Fig. 6). The energy barrier is only 0.70 eV by VASP and 0.80eV by CASTEP.[40] Both values are close to the result of 0.68 eV calculated by Duan *et al*,[24] and are also comparable with the horizontal migration barrier of 0.83 eV for Al in Ti_2AlC[21-23], 0.53 eV for Cd in Ti_2CdC, 0.63 eV for In in Ti_2InC, 0.66 eV for Sn in Ti_2SnC and 0.75 eV for Ga in Ti_2GaC.[41] This barrier is only slightly higher than the barrier for Al self-diffusion in bulk FCC Al (0.61eV),[42] but is much lower compared with the formation energy of bulk Al vacancy in Ti_2AlN (2.09~3.75 eV, Table 1). The large difference between vacancy formation energy and vacancy diffusion barrier may be attributed to bonding structure in Ti_2AlN, where the Al atom is bonded with 6 Ti atoms in a Ti_6Al prism. Formation of an Al vacancy requires breaking of 6 Ti-Al bonds completely, while diffusion of an Al atom does not need break Ti-Al bonds abruptly as Al can slip along the (0001) atomic plane with low resistance.[43]

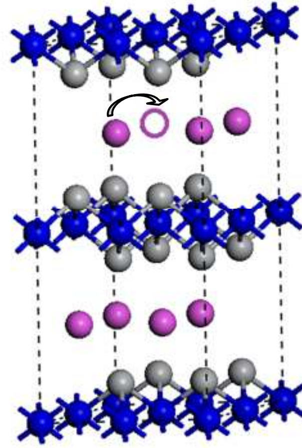

Fig. 6 Schematic drawing of an Al atom (pink ball) exchanging its position with a neighboring Al vacancy (pink empty ball) horizontally along (0001) Al plane. Grey and blue balls represent Ti and N atoms, respectively.

To compare the diffusion barriers along and across (0001) planes, three plausible routes for Al atoms' diffusion along the *c*-axis (Fig. 7) were selected for evaluation. Note that the exploration of potential vertical diffusion routes does not intend to be exhaustive but rather to give some representative values for comparison. In Fig. 7(a), we consider the first route assuming that Al atom at position 0 will jump to the position of Ti or N along *c*-axis where vacancy of Ti or N already exists. There are two possibilities for a Ti vacancy, either at position 1 (V_{Ti}^{1}) or 2 (V_{Ti}^{2}), while there is only one possibility (indicated as position 3) for N vacancy (V_{N}^{3}). The calculated energy barriers are 1.65eV from V_{Al}^{0} to V_{Ti}^{1}, 11.7 eV from V_{Al}^{0} to V_{Ti}^{2} and 8.87eV from V_{Al}^{0} to V_{N}^{3}. Hence, the energy barrier for the first jump in the diffusion of Al atom in route 1 is 1.65eV.

In Fig. 7(b), we consider route 2 assuming that there two vacancies (N and Al vacancies) which have been already created. The Al atom at 0 position (V_{Al}^{0}) will jump to position 1 (V_{N}^{1}) then jump to position 2 (V_{Al}^{2}). Calculations show that the energy barriers are 8.79 eV from V_{Al}^{0} to

V_N^1 and 1.98 eV from V_N^1 to V_{Al}^2. Hence, the energy barrier for the first jump in the diffusion of Al atom in route 2 is 8.79eV.

In Fig. 7(c), we consider route 3 assuming that there are two vacancies (Ti and Al vacancies) initially in the 2 × 2 × 1 supercell. The Al vacancy at 0 position (V_{Al}^0) will jump to position 1 (V_{Ti}^1) then jump to position 2 (V_{Al}^2). Calculations show that the energy barriers are 11.54 eV from V_{Al}^0 to V_{Ti}^1 and 0.25 eV from V_{Ti}^1 to V_{Al}^2. Hence, the energy barrier for the first jump in the diffusion of Al atom in route 3 is 11.54 eV.

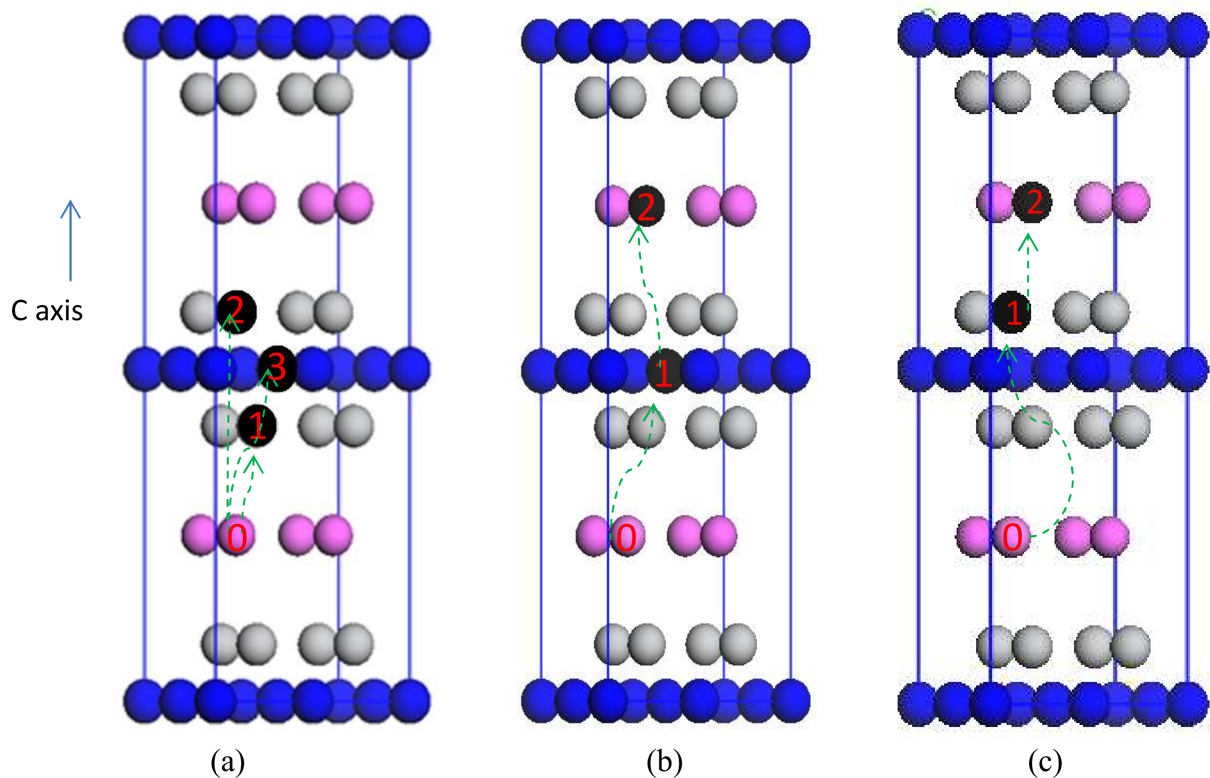

Fig. 7 Three different routes for Al atoms (pink ball) to diffuse out of Ti_2AlN along *c*-axis across Ti layer (grey ball) and N layer (blue ball).

Although the Al atom jumps to the same position of V_N^3 in route 1 (Fig. 7(a)) and V_N^1 in route 2 (Fig. 7(b)), the diffusion barriers are slightly different between route 1 (8.87 eV) and route 2 (8.79 eV) due to the different number of vacancies in the initial structures (one vacancy

in route 1 and two vacancies in route 2). Same reason also leads to a slightly different diffusion barrier for Al atom to jump to V_{Ti}^{2} in route 1 and V_{Ti}^{1} in route 3. Nevertheless, the present calculation clearly shows that the Al atom's migration barrier is much larger across than along (0001) plane, even without considering the prerequisite vacancy formation energy. Al has similarly been reported to have low migration barrier (0.83 eV) and high diffusivity along (0001) plane inside Ti_2AlC,[21-23] which help interpret the experimental observed rapid out-diffusion of Al during decomposition of Ti_2AlC at high temperatures and formation of Al_2O_3 scale during oxidation of Ti_2AlC. We have also observed surface segregation of Al at 700°C and desorption of Al from Ti_2AlN above 800°C during annealing of Ti_2AlN thin film in ultra-high-vacuum condition.[18] These observation can now be quantitatively understood by the low Al diffusion barrier via vacancy jump along (0001) plane in Ti_2AlN, which could also lead to Al_2O_3 layer formation during oxidation of Ti_2AlN, improving the oxidation resistance of Ti_2AlN.[5]

IV. Conclusion

In summary, DFT calculations have been carried out to understand the theoretical origin of Al deficient Ti_2AlN which we have observed experimentally. Vacancy formation energy calculations showed that Al vacancy should be the dominant vacancy type in N-rich Ti_2AlN, since it requires the lowest formation energies not only at top surface layer (1.05 eV) and second surface layer (2.70 eV), but also in bulk (2.09~3.75 eV), when compared with the respective formation energies for Ti and N vacancies at the same location. The Al deficient sub-stoichiometric Ti_2Al_xN can retain the MAX phase structure after losing a maximum of 25% Al atoms. Al vacancy can assist Al atoms diffuse along (0001) plane with a low energy barrier of 0.80 eV, in comparison with a high energy barrier between 1.65 and 11.54 eV for the first jump

during diffusion across (0001) plane. This work helps quantitatively explain the structural tolerance of Ti_2AlN to Al vacancy both during growth process and after heavy ion irradiation, as well as the preferential surface segregation of Al during high temperature annealing of Ti_2AlN.

- AUTHOR INFORMATION

Corresponding Authors:

*Tel.: +65-64191332

*Fax: +65-64632536

*E-mail address: jinhm@ihpc.a-star.edu.sg

**Tel.: +65-68748184

**Fax: +65-67744657

**E-mail address: sj-wang@imre.a-star.edu.sg

- **Acknowledgment**

This project was funded by Science and Engineering Research Council (SERC) and supported by Aerospace Program of A*STAR (Grant No: 112 155 0512).

- **Supporting Information**

Supporting Information Available: the schematic process of removing 2, 4, 6, 8, 9, 10 and 12 Al atoms from a perfect 4 × 4 × 1 Ti_2AlN, as well as related gradual development of the total density of states (TDOS) and partial density of states (PDOS) of Ti, N and Al. This material is available free of charge via the Internet at http://pubs.acs.org.

- **References**

(1) Barsoum, M. W., The $M_{n+1}AX_n$ Phases: A New Class of Solids; Thermodynamically Stable Nanolaminates. *Prog. Solid State Chem.* **2000**, *28*, 201-281.
(2) Eklund, P.; Beckers, M.; Jansson, U.; Hogberg, H.; Hultman, L., The $M_{n+1}AX_n$ Phases: Materials Science and Thin-film Processing. *Thin Solid Films* **2010**, *518*, 1851-1878.
(3) Cabioc'h, T.; Eklund, P.; Mauchamp, V.; Jaouen, M., Structural Investigation of Substoichiometry and Solid Solution Effects in $Ti_2Al(C_x,N_{1-x})_y$ Compounds. *J. Eur. Ceram. Soc.* **2012**, *32*, 1803-1811.
(4) Procopio, A. T.; El-Raghy, T.; Barsoum, M. W., Synthesis of Ti_4AlN_3 and Phase Equilibria in the Ti-Al-N System. *Metall. Mater. Trans. A* **2000**, *31*, 373-378.
(5) Cui, B.; Sa, R.; Jayaseelan, D. D.; Inam, F.; Reece, M. J.; Lee, W. E., Microstructural Evolution During High-temperature Oxidation of Spark Plasma Sintered Ti_2AlN Ceramics. *Acta Mater.* **2012**, *60*, 1079-1092.
(6) Naguib, M.; Mashtalir, O.; Carle, J.; Presser, V.; Lu, J.; Hultman, L.; Gogotsi, Y.; Barsoum, M. W., Two-Dimensional Transition Metal Carbides. *ACS Nano* **2012**, *6*, 1322-1331.
(7) Frodelius, J.; Eklund, P.; Beckers, M.; Persson, P. O. A.; Hogberg, H.; Hultman, L., Sputter Deposition from a Ti_2AlC Target: Process Characterization and Conditions for Growth of Ti_2AlC. *Thin Solid Films* **2010**, *518*, 1621-1626.
(8) Eklund, P.; Beckers, M.; Frodelius, J.; Hogberg, H.; Hultman, L., Magnetron Sputtering of Ti_3SiC_2 Thin Films from a Compound Target. *J. Vac. Sci. Technol.,A* **2007**, *25*, 1381-1388.
(9) Wilhelmsson, O.; Eklund, P.; Hogberg, H.; Hultman, L.; Jansson, U., Structural, Electrical and Mechanical Characterization of Magnetron-sputtered V-Ge-C Thin Films. *Acta Mater.* **2008**, *56*, 2563-2569.
(10) Emmerlich, J.; Eklund, P.; Rittrich, D.; Hogberg, H.; Hultman, L., Electrical Resistivity of $Ti_{n+1}AC_n$ (A = Si, Ge, Sn, n=1-3) Thin Films. *J. Mater. Res.* **2007**, *22*, 2279-2287.
(11) Whittle, K. R.; Blackford, M. G.; Aughterson, R. D.; Moricca, S.; Lumpkin, G. R.; Riley, D. P.; Zaluzec, N. J., Radiation Tolerance of $M_{n+1}AX_n$ Phases, Ti_3AlC_2 and Ti_3SiC_2. *Acta Mater.* **2010**, *58*, 4362-4368.
(12) Nappe, J. C.; Grosseau, P.; Audubert, F.; Guilhot, B.; Beauvy, M.; Benabdesselam, M.; Monnet, I., Damages Induced by Heavy Ions in Titanium Silicon Carbide: Effects of Nuclear and Electronic Interactions at Room Temperature. *J. Nucl. Mater.* **2009**, *385*, 304-307.
(13) Xiao, J.; Yang, T.; Wang, C.; Xue, J.; Wang, Y., Investigations on Radiation Tolerance of $M_{n+1}AX_n$ Phases: Study of Ti_3SiC_2, Ti_3AlC_2, Cr_2AlC, Cr_2GeC, Ti_2AlC, and Ti_2AlN. *J. Am. Ceram. Soc.* **2015**, *98*, 1323-1331.
(14) Bugnet, M.; Cabioc'h, T.; Mauchamp, V.; Guerin, P.; Marteau, M.; Jaouen, M., Stability of the Nitrogen-deficient Ti_2AlN_x MAX Phase in Ar^{2+}-irradiated (Ti,Al)N/Ti_2AlN_x Multilayers. *J. Mater. Sci.* **2010**, *45*, 5547-5552.
(15) Tallman, D. J.; Hoffman, E. N.; Caspi, E. a. N.; Garcia-Diaz, B. L.; Kohse, G.; Sindelar, R. L.; Barsoum, M. W., Effect of Neutron Irradiation on Select MAX Phases. *Acta Mater.* **2015**, *85*, 132-143.
(16) Sickafus, K. E.; Minervini, L.; Grimes, R. W.; Valdez, J. A.; Ishimaru, M.; Li, F.; McClellan, K. J.; Hartmann, T., Radiation Tolerance of Complex Oxides. *Science* **2000**, *289*, 748-751.
(17) Zhang, Z.; Nie, Y.; Shen, L.; Chai, J.; Pan, J.; Wong, L. M.; Sullivan, M. B.; Jin, H.; Wang, S. J., Charge Distribution in the Single Crystalline Ti_2AlN Thin Films Grown on MgO(111) Substrates. *J. Phys. Chem. C* **2013**, *117*, 11656-11662.

(18) Zhang, Z.; Jin, H.; Chai, J.; Shen, L.; Seng, H. L.; Pan, J.; Wong, L. M.; Sullivan, M. B.; Wang, S. J., Desorption of Al and Phase Transformation of Ti_2AlN MAX Thin Film upon Annealing in Ultra-High-Vacuum. *J. Phys. Chem. C* **2014**, *118*, 20927-20939.
(19) Wang, X. H.; Zhou, Y. C., High-temperature Oxidation Behavior of Ti_2AlC in Air. *Oxid. Met.* **2003**, *59*, 303-320.
(20) Basu, S.; Obando, N.; Gowdy, A.; Karaman, I.; Radovic, M., Long-Term Oxidation of Ti_2AlC in Air and Water Vapor at 1000-1300°C Temperature Range. *J. Electrochem. Soc.* **2012**, *159*, C90-C96.
(21) Wang, J.; Zhou, Y.; Liao, T.; Zhang, J.; Lin, Z., A First-principles Investigation of the Phase Stability of Ti_2AlC with Al Vacancies. *Scr. Mater.* **2008**, *58*, 227-230.
(22) Liao, T.; Wang, J.; Zhou, Y., Ab Initio Modeling of the Formation and Migration of Monovacancies in Ti_2AlC. *Scr. Mater.* **2008**, *59*, 854-857.
(23) Tan, J.; Han, H.; Wickramaratne, D.; Liu, W.; Zhao, M.; Huai, P., A Comparative First-principles Study of the Electronic, Mechanical, Defect and Acoustic Properties of Ti_2AlC and Ti_3AlC. *J. Phys. D: Appl. Phys.* **2014**, *47*, 215301.
(24) Duan, J. Z.; Zhang, J. R.; Wang, C. L.; Qiu, Y.; Duan, W. S.; Yang, L., First Principles Investigation of Point Defect-related Properties in Ti_2AlN. *Rsc Advances* **2014**, *4*, 42014-42021.
(25) Rawn, C. J.; Barsoum, M. W.; El-Raghy, T.; Procipio, A.; Hoffmann, C. M.; Hubbard, C. R., Structure of Ti_4AlN_3 - A Layered $M_{n+1}AX_n$ Nitride. *Mater. Res. Bull.* **2000**, *35*, 1785-1796.
(26) Music, D.; Ahuja, R.; Schneider, J. M., Theoretical Study of Nitrogen Vacancies in Ti_4AlN_3. *Appl. Phys. Lett.* **2005**, *86*, 031911.
(27) Kresse, G.; Hafner, J., Ab-Initio Molecular-Dynamics Simulation of the Liquid-Metal Amorphous-Semiconductor Transition in Germanium. *Phys. Rev. B* **1994**, *49*, 14251-14269.
(28) Perdew, J. P.; Burke, K.; Ernzerhof, M., Generalized Gradient Approximation Made Simple. *Phys. Rev. Lett.* **1996**, *77*, 3865-3868.
(29) Blochl, P. E., Projector Augmented-Wave Method. *Phys. Rev. B* **1994**, *50*, 17953-17979.
(30) *"Materials Studio"*, Accelrys Software Inc.: 2001-2011.
(31) Zhou, Y. C.; Sun, Z. M., Electronic Structure and Bonding Properties of Layered Machinable $T_{i2}AlC$ and Ti_2AlN Ceramics. *Phys. Rev. B* **2000**, *61*, 12570-12573.
(32) Lin, Z. J.; Zhuo, M. J.; Li, M. S.; Wang, J. Y.; Zhou, Y. C., Synthesis and Microstructure of Layered-ternary Ti_2AlN Ceramic. *Scr. Mater.* **2007**, *56*, 1115-1118.
(33) Yang, Y.; Keunecke, M.; Stein, C.; Gao, L. J.; Gong, J.; Jiang, X.; Bewilogua, K.; Sun, C., Formation of Ti_2AlN Phase After Post-heat Treatment of Ti-Al-N films Deposited by Pulsed Magnetron Sputtering. *Surf. Coat. Technol.* **2012**, *206*, 2661-2666.
(34) Dolique, V.; Jaouen, M.; Cabioc'h, T.; Pailloux, F.; Guérin, P.; Pélosin, V., Formation of (Ti,Al)N / Ti_2AlN Multilayers After Annealing of TiN / TiAl(N) Multilayers Deposited by Ion Beam Sputtering. *J. Appl. Phys.* **2008**, *103*, 083527.
(35) Scabarozi, T.; Ganguly, A.; Hettinger, J. D.; Lofland, S. E.; Amini, S.; Finkel, P.; El-Raghy, T.; Barsoum, M. W., Electronic and Thermal Properties of $Ti_3Al(C_{0.5},N_{0.5})_2$, $Ti_2Al(C_{0.5},N_{0.5})$ and Ti_2AlN. *J. Appl. Phys.* **2008**, *104*, 073713.
(36) Joelsson, T.; Flink, A.; Birch, J.; Hultman, L., Deposition of Single-crystal Ti_2AlN Thin Films by Reactive Magnetron Sputtering from a 2Ti : Al Compound Target. *J. Appl. Phys.* **2007**, *102*, 074918.
(37) Beckers, M.; Schell, N.; Martins, R. M. S.; Mucklich, A.; Moller, W.; Hultman, L., Nucleation and Growth of Ti_2AlN Thin Films Deposited by Reactive Magnetron Sputtering onto MgO(111). *J. Appl. Phys.* **2007**, *102*, 074916.

(38) Persson, P. O. A.; Kodambaka, S.; Petrov, I.; Hultman, L., Epitaxial $Ti_2AlN(0001)$ Thin Film Deposition by Dual-target Reactive Magnetron Sputtering. *Acta Mater.* **2007**, *55*, 4401-4407.
(39) Mo, Y. X.; Rulis, P.; Ching, W. Y., Electronic Structure and Optical Conductivities of 20 MAX-phase Compounds. *Phys. Rev. B* **2012**, *86*, 165122.
(40) We have seperately calcaulted the diffusion barriers along the (0001) planes for Ti and N vacancies to be 2.7 and 2.9 eV, respectively, by CASTEP.
(41) Liu, B.; Wang, J. Y.; Zhang, J.; Wang, J. M.; Li, F. Z.; Zhou, Y. C., Theoretical Investigation of A-element Atom Diffusion in Ti_2AC (A=Sn, Ga, Cd, In, and Pb). *Appl. Phys. Lett.* **2009**, *94*, 181906.
(42) Ortega, M. G.; de Debiaggi, S. B. R.; Monti, A. M., Self-diffusion in FCC Metals: Static and Dynamic Simulations in Aluminium and Nickel. *Phys. Status Solidi B-Basic Res.* **2002**, *234*, 506-521.
(43) Liao, T.; Wang, J.; Zhou, Y., Deformation Modes and Ideal Strengths of Ternary Layered Ti_2AlC and Ti_2AlN from First-principles Calculations. *Phys. Rev. B* **2006**, *73*, 214109.

Table of Contents (TOC) Image